Mesenchymal stem cells from cortical bone demonstrate increased clonal incidence, potency, and developmental capacity compared to their bone marrow–derived counterparts

Daniel Blashki[1,2], Matthew B Murphy[1,3], Mauro Ferrari[3], Paul J Simmons[1] and Ennio Tasciotti[3]

Abstract

In this study, we show that matrix dense cortical bone is the more potent compartment of bone than bone marrow as a stromal source for mesenchymal stem cells as isolated from adult rats. Lineage-depleted cortical bone-mesenchymal stem cells demonstrated >150-fold enrichment of colony forming unit–fibroblasts per cell incidence. compared to lineage-depleted bone marrow-mesenchymal stem cells, corresponding to a 70-fold increase in absolute recovered colony forming unit–fibroblasts. The composite phenotype $Lin^-/CD45^-/CD31^-/VLA-1^+/Thy-1^+$ enriched for clonogenic mesenchymal stem cells solely from cortical bone–derived cells from which 70% of clones spontaneously differentiated into all lineages of bone, cartilage, and adipose. Both populations generated vascularized bone tissue within subcutaneous implanted collagen scaffolds; however, cortical bone–derived cells formed significantly more osteoid than bone marrow counterparts, quantified by histology. The data demonstrate that our isolation protocol identifies and validates mesenchymal stem cells with superior clonal, proliferative, and developmental potential from cortical bone compared to the bone marrow niche although marrow persists as the typical source for mesenchymal stem cells both in the literature and current pre-clinical therapies.

Introduction

Mesenchymal stem cells (MSCs) were initially isolated from the bone marrow (BM) and described as rare, adherent colony forming cells in culture.[1] "Colony forming unit–fibroblasts" (CFU-F) have since been a measure for stem and precursor cells in vitro and are now often synonymous with the term MSC although equivalent or similar cell populations are given alternate names such as mesenchymal stromal cells and multipotent progenitor cells. In the context of this study, MSC is used for all isolated stromal candidate fractions, in keeping with the literature. MSCs

[1]Center for Stem Cell Research, The University of Texas Health Science Center at Houston, Houston, TX, USA
[2]Department of Immunology, The University of Melbourne, Parkville, VIC, Australia
[3]Department of Nanomedicine, The Methodist Hospital Research Institute, Houston, TX, USA

Corresponding author:
Daniel Blashki, Department of Immunology, The University of Melbourne, Peter Doherty Institute for Infection and Immunity 792 Elizabeth Street Melbourne, 3000, VIC, Australia.
Email: daniel.blashki@unimelb.edu.au

occupy several roles within their native environment; most critically, they provide a structural and signaling "niche" to the resident marrow hematopoietic system and additionally maintain a capacity to differentiate to the predominant tissue lineages of mesoderm. Their study within the stem cell and regenerative medicine fields has expanded for the past four decades with burgeoning interest, relating to their diverse array of proliferative, developmental, and immuno-suppressive properties;[2–4] consequently, they are a prime candidate for a host of clinical therapies. Although various organ sites and harvesting methods have now been extensively reported,[5,6] the original isolation procedure with BM aspirates/flushes currently and continuously persists as the predominant system for generating MSCs.

MSCs are incorporated into numerous recruiting and active clinical trials;[7,8] however, this frequently occurs without full knowledge of the breadth in potential of the cells utilized; questions remain on the native identity and origin of MSCs. BM currently persists as the dominant location to harvest MSCs; cells are typically derived by one-step isolation methodologies of gradient density centrifugation or plastic adherence in cell culture, to separate stromal cells from the hematopoietic bulk and often do not utilize surface markers for immunophenotypic separation. For cultured MSCs (irrespective of isolation strategy), there is a surface marker consensus with expression of CD73, CD90, CD44, and CD105, and a lack of CD11b, CD14, CD34, CD45, and CD79a.[7,9] However, no such agreement exists over the correct composite marker panel to define MSCs in freshly isolated (non-cultured) populations, as such these markers were not all readily incorporated within our studies, as the focus was toward prospective isolation of fresh, not cultured cells.

Unlike BM-MSCs, relatively little characterization has been reported on MSCs isolated from the neighboring yet anatomically and histologically distinct cortical bone (CB) tissue.[10] Limited publications have reported that the most potent stem and osteo-progenitor cells reside within CB rather than the surrounding periosteum or adjacent BM.[11,12] Accordingly, we developed a methodology to physically isolate stromal cells from the CB and prospectively fractionate them by surface antigen expression in order to assess the resulting fractions as putative MSC candidates. We also compared unfractionated, mononuclear, and lineage-depleted cell populations harvested from the neighboring compartments of BM and CB within the same animal, with respect to primary and secondary CFU-F incidence, with studies on tri-lineage mesodermal differentiation potential and de novo bone formation in vivo. A critical outcome of these studies for the MSC field is the demonstration that BM is not necessarily the better source of MSCs with regard to cell incidence and potency; given the almost ubiquitous use of marrow for harvest or purchase of MSCs, this study serves as a comparative evaluation. The results show that BM can produce a subset of clonogenic, multi-lineage cells; however, they are out-numbered and outperformed by an equivalent harvest of CB-MSCs. The significance of these data is that BM should perhaps not be the automatic default source for MSCs in pre-clinical studies and clinical translation of cell therapy.

Results

Isolation of stromal cells from the CB and BM compartments of long bones

The BM and CB physically reside within a shared space of bone as adjacent compartments (Figure 1(a)) and were isolated into separate cell fractions in this study. As shown in Figure 1(b), a 1-h enzymatic digest was sufficient to liberate cells embedded within the dense bone extracellular matrix (ECM), observed by a majority of empty lacunae lacking nuclei. The edge of the digested piece on the right also indicates the abraded bone edge following earlier removal of the periosteum. For the purpose of the study and to normalize cell counts and colony scoring, a standard harvest of bones, as "per rat" isolation designates the four long leg bones: two femora and two tibiae. Across the male rats employed in the studies, the mean mass of bone isolated per rat from the four leg bones was $1.10 \pm 0.11\,g$ ($n=6$). The mean cell yield per rat of total bone marrow (TBM) was $719 \times 10^6 \pm 82.4$ ($n=8$), a significant ($p<0.05$) 56-fold greater number than the mean yield of total cortical bone (TCB) of $12.8 \times 10^6 \pm 2.1$ (Table 1).

CB-MSCs demonstrate a higher incidence of CFU-F than their BM-derived counterparts

Cells from CB and BM were seeded in a serial density gradient to assess their capacity for clonal proliferation. At each density, CB-MSCs produced significantly more CFU-F than the BM-derived cells ($p<0.01$, Figure 1(c)), averaging a 15-fold greater quantity (ranging from 9- to 21-fold with 95% confidence intervals). The appearance of the CB-derived colonies is also shown in Figure 1(c) demonstrating the heterogeneous size range of CFU-F. The isolation from the compartments of bone involved enrichment for relative incidence of clonogenic cells, summarized in Figure 1(d), with seeding of 500,000 cells in six-well plates across the sequentially enriched fractions. A slight increase in the number of colonies was observed in the Ficoll separated mononuclear cells (BM-MNC) and Ficoll and lineage-depleted (Lin−) fractions of the BM, yet not significant and with a cell loss of >90%. Conversely, the CB-MSCs demonstrated an enrichment of CFU-F; the Lin− fraction with a 90% depletion produced a significant fivefold increase in CFU-F (❀ $p<0.05$). In addition, both CB fractions showed a significantly greater colony forming capacity compared to all BM fractions (✳ $p<0.01$). The yield of
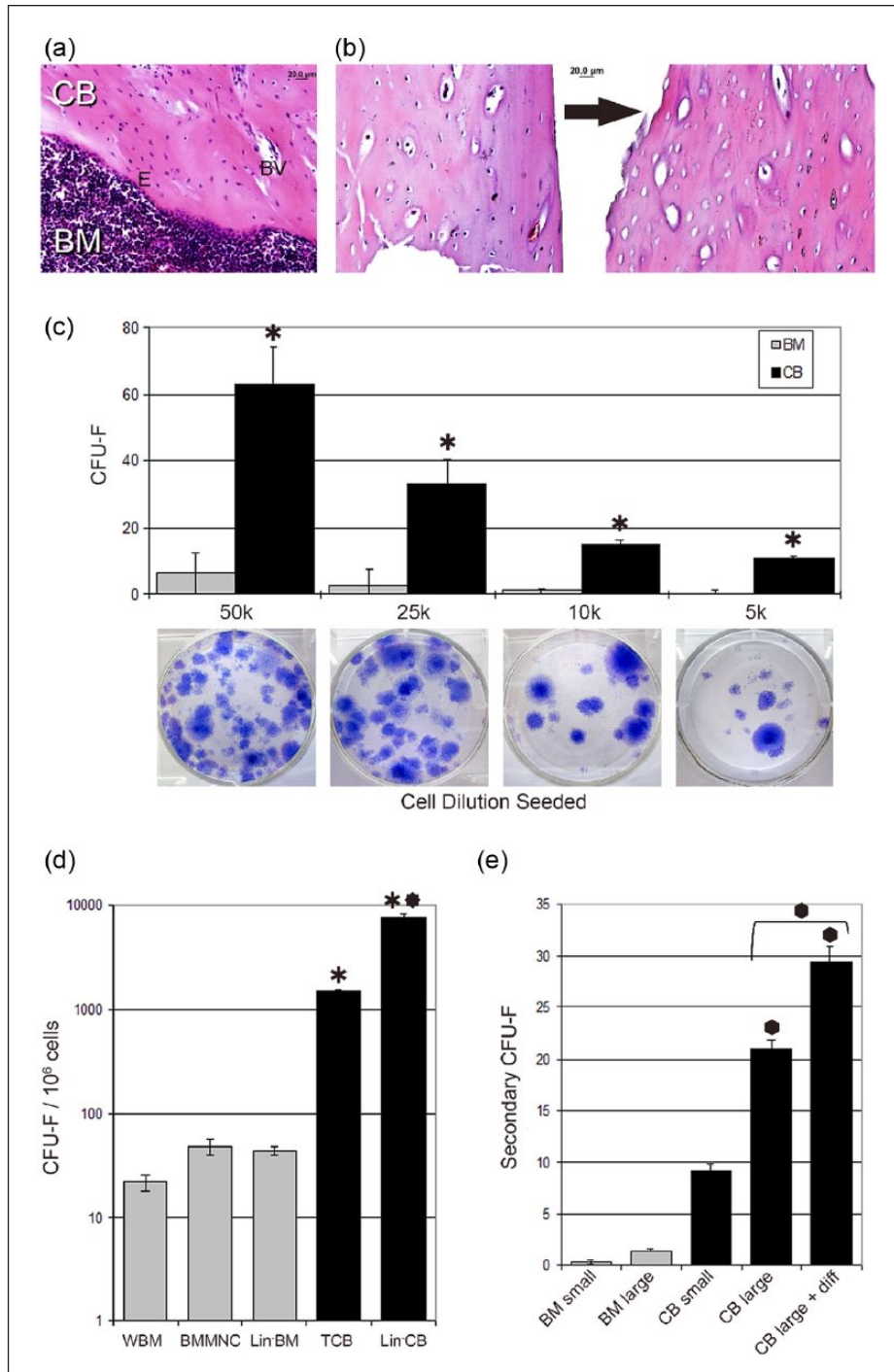
Figure 1. The BM and CB compartments and incidence of primary and secondary CFU-F. (a) H&E stain of femur showing adjacent CB and BM compartments of bone. The BM is dense with nuclei, contrasted with the matrix dense CB, including a row of endosteal cells (e) contiguous with the BM and perivascular cells surrounding the blood vessels (BV) (20×). (b) Crushed bone chip pieces pre- and post-enzymatic digestion; arrow points to the abraded bone edge on a post-digestion piece (20×, scale bar: 20 µm). (c) Incidence of CFU-F from BM-MNC versus CB-derived cells at varying seeding doses 5000–50,000 per well (six-well plate). Representative images of CB CFU-F stained with toluidine blue are shown. (d) CFU-F count per 10^6 cells isolated from each cell fraction. A total of 500,000 cells were seeded in six-well plates and results are reported as mean value ± SEM (n = 3). (e) Incidence of secondary colonies from re-plated primary CFU-F. Counts represent mean value ± SEM (n = 8) per six-well plate comprising 25% of the primary CFU-F (statistical significance: ✱p < 0.01, ✿p < 0.05, ●p < 0.001).
WBM: whole (total) bone marrow; BM-MNC: Ficoll bone marrow mononuclear cells; Lin⁻BM: antibody cocktail lineage–depleted bone marrow-mononuclear cells; TCB: total cortical bone; Lin⁻CB: antibody cocktail lineage–depleted cortical bone.

Table 1. Cell yield and CFU-F incidence of isolated fractions from BM and CB.

Cell fraction	Cells/rat ($\times 10^6$)	CFU-F/10^6 cells	CFU-F/rat
Total BM	719.0 ± 82.4	21.8 ± 3.95	15,674.2
Ficoll BM MNC	72.1 ± 12.3	48.2 ± 9.14	3475.2
Ficoll and Lin⁻ BM MNC	3.1 ± 0.3	44.0 ± 4.00	136.4
Total CB	12.8 ± 2.1	1488.9 ± 67.59	19,057.9
Lin⁻ CB MNC	1.4 ± 0.2	7633.3 ± 638.4	10,686.6

CFU-F: colony forming unit–fibroblasts; BM: bone marrow; CB: cortical bone; MNC: mononuclear cells.
Cell counts are mean value $\pm$ standard error of mean (SEM; n = 8 harvests, excepting n = 4 for the Lin⁻ fractions). One rat harvest = four long bones: two tibiae and two femora. CFU-F counts are mean value $\pm$ SEM (n = 3) with triplicate repeats per fraction. Counts are per 10^6 cells harvested and expressed as CFU-F/rat for absolute recovery of CFU-F (total: unmodified cell isolate; Ficoll: following density spin; MNC: mononuclear cells; Lin⁻: following bead-based immunomagnetic removal; lineage marker depleted cell fraction: (CD2, CD3, CD4, CD8, CD18, CD11b/c, CD45RA, CD71, Gr(RP-1), and Mono/Mac)).

cells in each fraction and their respective CFU-F capacity are summarized in Table 1, which shows the absolute number of CFU-F per rat long bones. TBM has ~50-fold more cells than TCB; however, the CB-derived cells demonstrate a ~70-fold greater enrichment of CFU-F. The sequential depletion within BM produces a stromal cell-rich isolate yet does not result in an equivalent enrichment for colony forming cells, with 80% CFU-F lost. However, the Lin⁻CB which comprises 11% of the TCB yield still retains just over 50% of CFU-F, a robust enrichment for candidate MSCs from bone tissue itself. CB cells showed a significantly enhanced capacity to form secondary clones over all BM cells (Figure 1(e), ⬤p < 0.001). Small-sized primary CB CFU-F successfully re-plated several fold greater than the largest of BM-derived colonies, indicating that the primary determinant for serial clones is the compartment of origin. There was a clear impact of the primary colony size on the ability to initiate secondary colony formation; large primary CFU-F were significantly more capable after re-plating than small primary CFU-F (⬤p < 0.001), and the large and differentiating CFU-F produced more secondary colonies than large non-differentiating CFU-F (⬤p < 0.001).

Primary CFU-F from CB are larger and spontaneously differentiate to mesodermal lineages compared to their BM-derived counterparts

A qualitative difference was observed in the size and composition of CFU-F from the two compartments; colonies from CB (Figure 2(a)) were larger than those from BM (Figure 2(b)), which was due to the cellularity, size, and morphology within the colony. Scoring CFU-F across seeding densities (n = 5) showed that a range from 5% to 40% of CB-derived CFU-F were scored as large; however, BM-derived CFU-F considered large were never greater than 5% of the total colony count. Morphological differences between the CB- and BM-derived CFU-F revealed a dense core and gradient within select colonies, with cells differentiating toward combinations of bone, cartilage, and

fat lineages (Figure 2(c); phase images, two-dimensional (2D); stained images). In all, 89% of the CB-derived CFU-F produced tri-calcium phosphate bone mineral shown by brown von Kossa positive regions. In all, 76% contained cobblestone cores with proteoglycan cartilage ECM shown by the alcian blue stain. Totally, 32% showed lipid accumulation revealed by the Oil Red O stain. The relative incidence of these spontaneously differentiating CFU-F indicated that BM-MNC were reduced in this capacity, whereas CB-derived CFU-F were more readily capable of differentiating (Figure 2(e)). An interesting feature of these data was the diminishing proportion of primary CFU-F that would differentiate as the seeding density of CB cells increased. At 5000 cells per six-well plate (~520 cells/cm²) up to 41% of CFU-F demonstrated this capacity; however, as the cell seeding approached 10-fold higher, the incidence was halved. This was primarily attributed to the growth surface area as a limiting factor and the contact with nearby colonies as an inhibitory regulation on proliferation. Conversely, a further order magnitude increase in cells was required just to observe the same phenomenon in BM.

CB-MSCs cells demonstrate comparatively enhanced tri-lineage differentiation potential

Additional experiments were performed to assess in vitro differentiation potential under well-established inductive conditions, which further demonstrated enhanced tri-lineage of CB-MSC. A series of inductive assays were performed on passage one BM- and CB-derived cells for 3 weeks, with summarized representative images shown in Figure 3. The osteogenic assays consistently demonstrated that CB-MSCs produced more mineral deposition than cells derived from BM (Figure 3(a)) as shown by von Kossa staining. Alkaline phosphatase (AP), an early-stage marker in bone differentiation, was present in both cell populations; however, higher activity was observed in the BM cell cultures, indicating that more cells were in early stages of the pathway as compared to CB, which
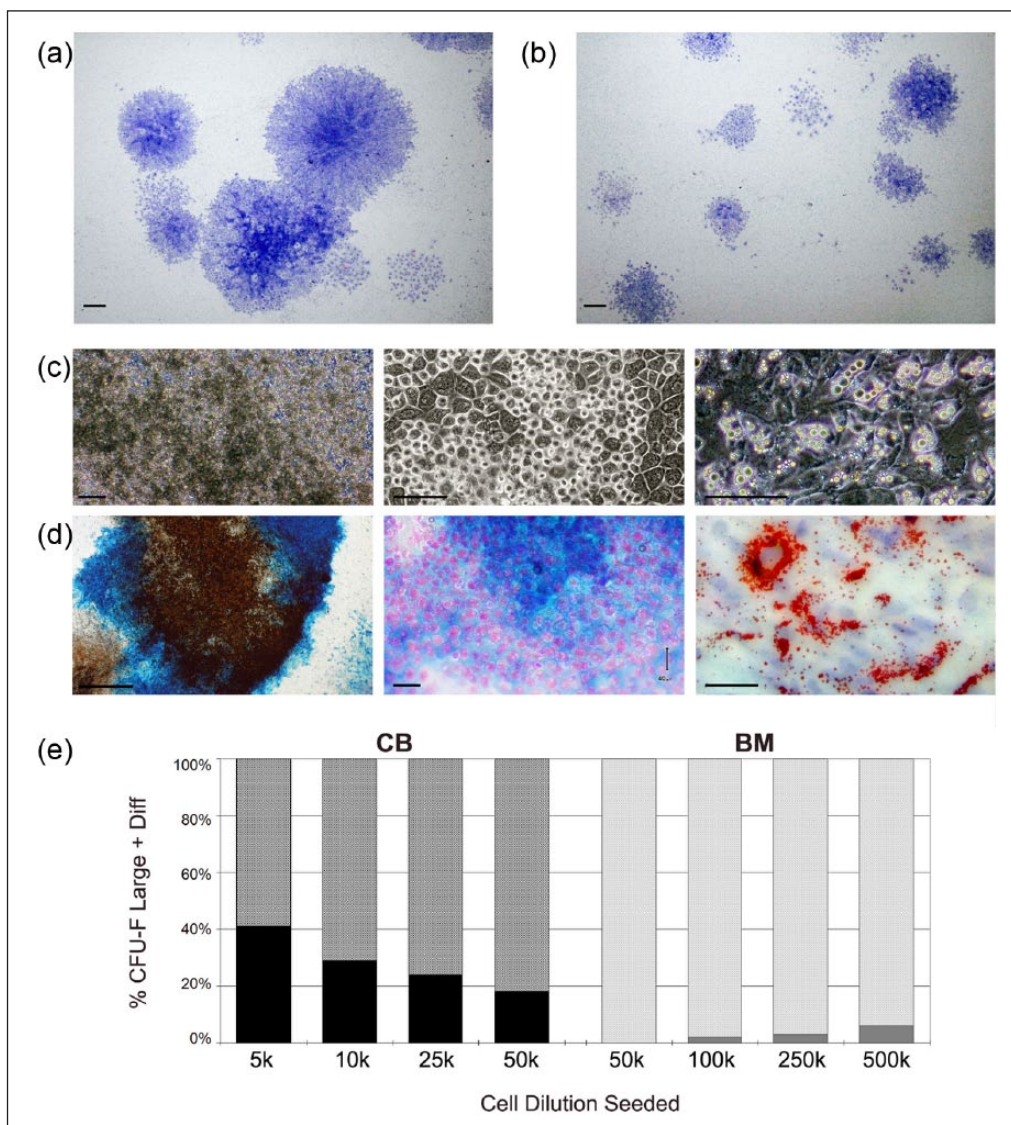
Figure 2. Primary CFU-F from CB are larger and spontaneously differentiate to mesodermal cell lineages as compared to their BM-derived counterparts. Low power magnification (1.5×, scale bars: 500 μm) images of (a) CFU-F of CB and (b) BM stained with toluidine blue. The emergence of spontaneous differentiation of CB colonies to mesodermal cell lineages: (c) phase microscopy of (L-R) bone, cartilage, adipose (20×, 40×, 40×, scale bars: 20 μm). (d) Stained cultures for bone; von Kossa (brown) and alkaline phosphatase (blue) (4×, scale bar: 100 μm), cartilage; alcian blue and nuclear fast red (20×, scale bar: 20 μm), adipose; Oil Red O and hematoxylin (40×, scale bar: 20 μm). (e) Relative percent incidence of spontaneously differentiating CFU-F in BM-MSCs and CB-MSCs (lower dark bars). Percentages are taken from the mean count of scored CFU-F at seeding densities of fresh cells at 5000–500,000 per six-well plate (n = 3).

had down-regulated AP expression as more committed osteogenic lineage markers became expressed. The potential of the CB-MSCs to differentiate toward the adipogenic lineage (Figure 3(b)) was demonstrated by the lipid filled spherical cytoplasmic vesicles and the more densely packed cuboidal cells and was confirmed by Oil red O staining. The production of lipids by early adipocytes was observed at lower frequencies in BM cultures, which contained more consistently fibroblastic, elongated cell morphology. Chondrogenic assays were performed in three-dimensional (3D) micromass pellet culture. Although both CB and BM produced micromass pellets that persisted over the assay period, CB-MSCs more successfully formed pellets that produced a robust cartilage matrix phenotype; 75% of CB-MSC-derived pellets produced a cartilage phenotype. The stains of sections revealed a matrix-rich core with more nuclei present around the outer layer. When stained with toluidine blue, regions of the matrix core displayed metachromasia in purple, indicating the acidic proteoglycans present in cartilage, confirmed by a stringent low pH alcian blue staining of the sulfated proteoglycans.
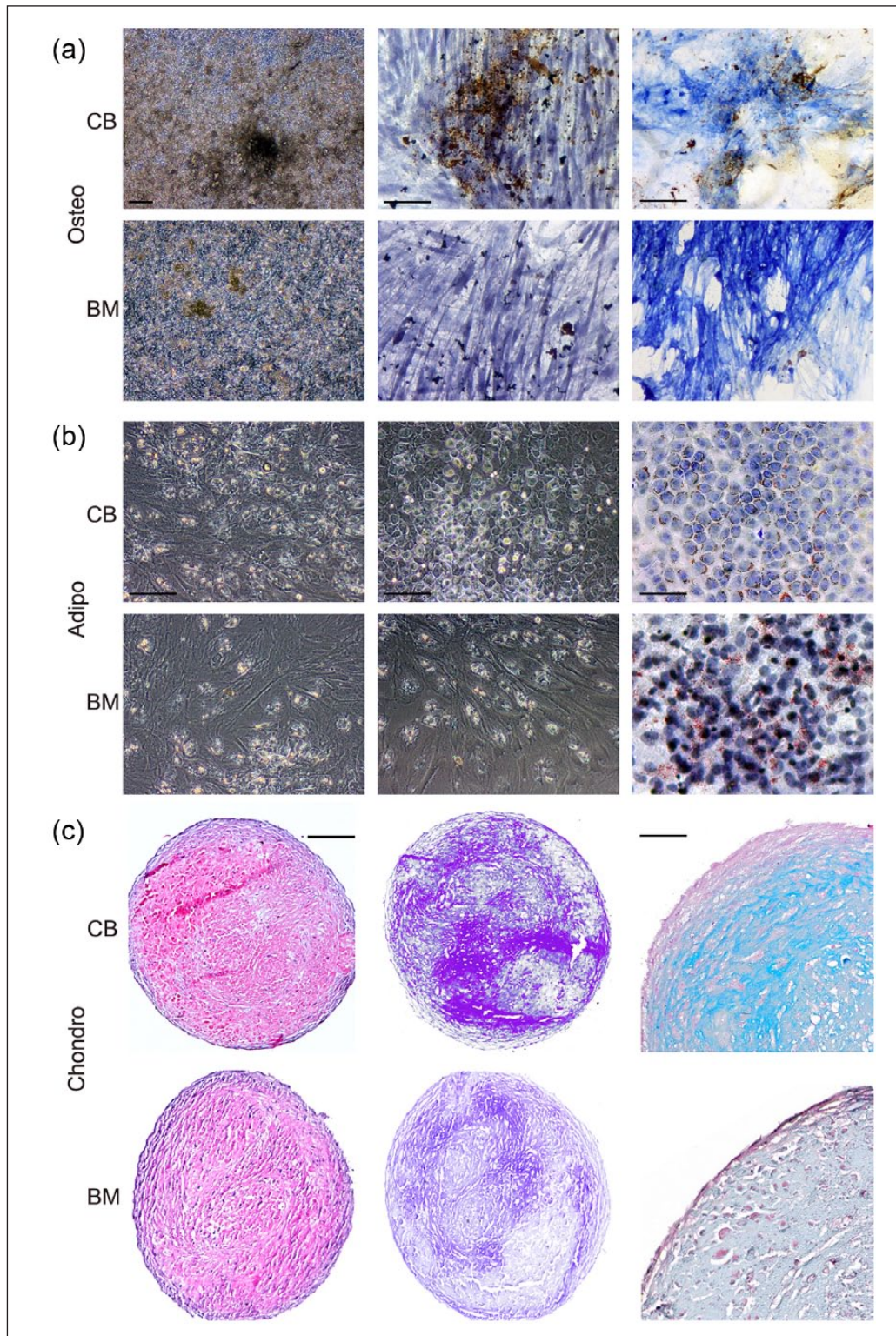
Figure 3. CB-derived cells demonstrate enhanced tri-lineage differentiation potential under inductive conditions. Comparison of passage one cells from CB and BM. (a) Osteogenic assay run for 20 days. The panels indicate mineral deposition by the cells (L-R) with a phase contrast image (10×), Von Kossa stain with hematoxylin (20×), and combined Von Kossa stain with AP in blue (20×, scale bars: 40 μm). (b) Adipogenic assay run for 20 days. (L-R) Phase contrast images at 10 and then 20 days (20×). At right is an Oil Red O stain for the lipid vesicles with hematoxylin (20×, scale bars: 40 μm). (c) Chondrogenic assay run for 21 days with sections of representative 3D pellets. (L-R) Hematoxylin and eosin stain (10×, scale bar: 80 μm), toluidine blue stain (10×), and alcian blue with nuclear fast red (20×, scale bar: 40 μm).
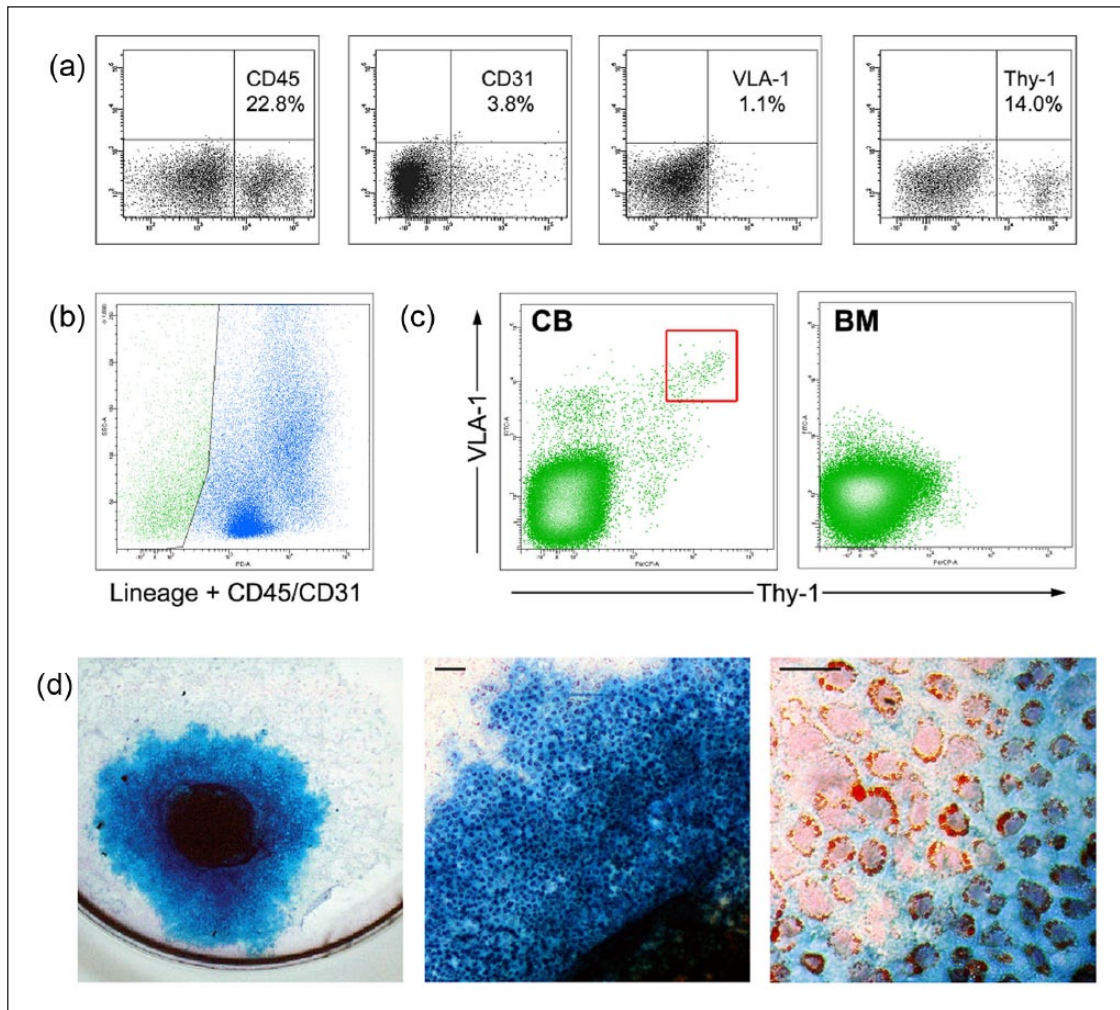
Figure 4. Immunophenotyping with surface markers reveals a clonogenic MSC population restricted to CB. (a) Representative FACS plots of CD45, CD31, VLA-1, and Thy-1 expression on freshly isolated CB cells, prior to any depletion. (b) Representative FACS plot for CB demonstrating the full "Lin⁻CD45⁻/CD31⁻" depletion of the combined lineage cocktail (10 hematopoietic lineage markers; (CD2, CD3, CD4, CD8, CD18, CD11b/c, CD45RA, CD71, Gr(RP-1), Mono/Mac)+CD45+CD31), with depleted cells gated on the left in green. (c) FACS plots of Thy-1 and VLA-1 labeling in the Lin⁻CD45⁻/CD31⁻ fractions of CB and BM, respectively. (d) Example CFU-F from CB-MSC of the Lin⁻/CD45⁻/CD31⁻/VLA-1⁺/Thy-1⁺ phenotype with spontaneous tri-lineage differentiation stained with von Kossa's reagent, alcian blue, and Oil Red O. Higher magnifications show three distinct stained regions (20×, scale bar: 40 μm) and the outer-edge adipose-cartilage boundary (40×, scale bar: 20 μm).

Immunophenotyping by fluorescence-activated cell sorting reveals an enriched MSC population restricted to the CB compartment

Stromal sub-populations were identified by fluorescence-activated cell sorting (FACS) using a combination of surface markers very late antigen 1 (VLA-1; CD49a, the α_1 integrin subunit) and Thy-1 (CD90), and the depletion of hematopoietic and endothelial cells. A lineage antibody cocktail was used in bead-based depletions (CD2, CD3, CD4, CD8, CD18, CD11b/c, CD45RA, CD71, Gr(RP-1), and Mono/Mac), labeling and removing committed cells based on a mouse panel previously described.[12] Additionally, isolates were labeled with CD45 and CD31

to redundantly remove hematopoietic and endothelial cells, respectively. Representative expression of the markers CD45, CD31, VLA-1, and Thy-1 on TCB isolated cells are shown in Figure 4(a). BM-MNC and TCB isolates were labeled with the 10-marker "Lin⁻" lineage cocktail, which identified 68.9% and 51.4% of the fractions, respectively. When combined with additional pan-leukocyte and endothelial markers, CD45 and CD31, these values rose to 98.3%±0.8% for BM and 90.8%±7.2% for CB, forming the complete lineage depletion panel: "Lin⁻CD45⁻/CD31⁻." An example plot of the lineage panel on CB cells is shown in Figure 4(b) with the gated Lin⁻CD45⁻/CD31⁻ fraction on the left. The relative proportion of Lin⁻ cells in the BM-MNC fraction was
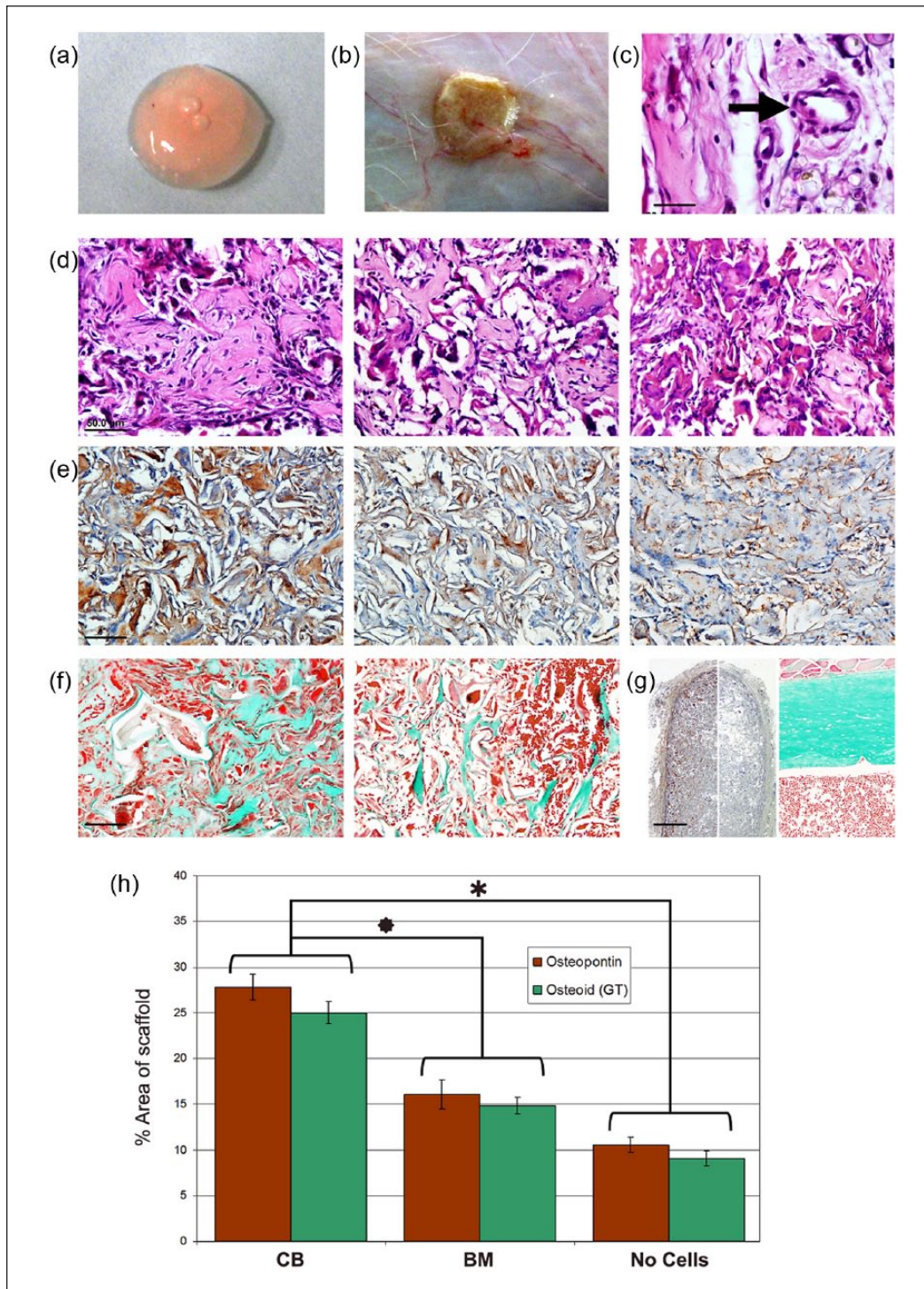
Figure 5. CB-derived cells contribute more to ectopic de novo bone tissue than BM-derived cells. (a) Example of the final gelated cell and biomaterial composite implant (1 cm diameter) ready for subcutaneous implantation and (b) an implant before excision, 4 weeks post-surgery. (c) H&E stain on a CB cell implant; arrow indicates an endogenously infiltrated blood vessel within the scaffold (40×, scale bar: 20 μm). Representative stains of implants, demonstrating formation of bone tissue in scaffolds: (d) H&E, (e) *OPN* immunostain. (L-R): CB, BM, no cells (20×, scale bar: 50 μm). (f) Representative Goldner's Trichrome stain on implants. (L-R): CB, BM (20×, scale bar: 40 μm). (g) Control stains (L) osteopontin positive and isotype negative on scaffolds and (R) Goldner's Trichrome on a femur (4×, scale bar: 100 μm). (h) Quantitation of bone tissue determined by osteopontin and Goldner's Trichrome stains as percentage of image area ± SEM (n = 3) (statistical significance: ✿$p < 0.05$, ❂$p < 0.001$).

considerably smaller (~40- to 50-fold) than that observed in the CB compartment. Total Thy-1 expression of Lin⁻ cells was observed in BM-MNC at 1.3%±1.1% compared with 19.4%±9.7% for CB, shown in Figure 4(a) in the representative plot at 14.0%. Combined, VLA-1 and Thy-1 labeled almost no Lin⁻ BM-MNC, whereas the CB contained several sub-populations (Figure 4(c)) including double-bright positive cells Lin⁻/CD45⁻/CD31⁻/VLA-1⁺/Thy-1⁺ (gated box in Figure 4(c)), a phenotype with an enriched capacity for spontaneously differentiating CFU-F at a frequency of 70% (Figure 4(d)). This phenotype had a low incidence (0.009%±0.005%) of Lin⁻ cells yet were the most enriched fraction in the bone, with ≥85% of the CFU-F scored as large. As shown in the higher magnification of the colony in Figure 4(d), the central regions of the colony showed differentiated cells in a morphological gradient with lipid containing cells at the outer edge, cartilage matrix–producing cells further in, and a dense mineralized core of bone differentiated cells.

CB-derived cells contribute more in the formation of ectopic de novo bone tissue when implanted subcutaneously

Low passage (≤P2) cells were loaded and gelated within porous collagen type-1 scaffolds (Figure 5(a)). Counts of non-incorporated cells following gelation revealed that 92%±4.6% of cells were retained within each scaffold. An example of a post-transplant scaffold prior to excision is shown in Figure 5(b), demonstrating robust neovascularization from the host animal to the implant. Figure 5(c) highlights an example of the blood vessels found within the majority of the implants—regardless of donor cell source or dose. Hematoxylin and eosin (H&E) stains of the implants indicated areas of bone tissue by the solid regions of light pink (Figure 5(d)). Among the implants it was observed that the most osteoid was produced in scaffolds injected with CB-derived cells, followed by those injected with BM-derived cells. Control implants with no cells yet retaining incorporated osteoinductive biomaterials such as BMP-2 (Bone morphogenetic protein 2) also contained small amounts of bone tissue. These observations were validated by quantification from micrographs with further stains; osteopontin (OPN) immunostaining identified newly made bone tissue (Figure 5(e)), and Goldner's Trichrome (GT) staining showed that the matrix observed was mature bone as indicated by the green regions (Figure 5(f)). A conclusive exhibition of the enhanced bone formation of cells derived from CB compared to BM was a quantitative analysis of the implants by image capture statistics of stained sections. As summarized in Figure 5(h), implants with CB-MSCs contained 25% area scored as bone, a significant result compared to 15% in implants containing BM-MSCs (✤p<0.05) or acellular implants (●p<0.001). No significant difference

was observed between BM-MSCs and acellular implants in terms of bone formation. As an indication of the robustness of the stains and image analysis, the percentage area detected as bone tissue positive within each group was concordant across the independent stains, with less than 15% difference in the values obtained for GT and OPN.

Discussion

This study represents an advance in the development of protocols for the isolation and purification of clonogenic MSCs from CB, demonstrating a superior biological capacity over their BM-derived counterparts—something infrequently observed or reported in existing literature. MSCs present an attractive cellular candidate in regenerative therapies for their robust multi-lineage differentiation capacity[13,14] combined with seemingly innate capacities to modulate inflammation, fight microbial bodies, and infection, and secrete a host of signaling cytokines.[15,16] Further evidence supporting the use of MSCs as a therapeutic agent in clinical applications include reported but as-yet not well elucidated immunosuppressive properties in allogeneic transplantation, and homing and migratory behavior to sites of tissue injury;[17–19] abilities mentioned here as commentary but not actively investigated in this study. Although BM remains the predominant, accepted source of putative MSCs for experimental and translational applications in regenerative medicine, our data demonstrate CB-MSCs with superior proliferative and differentiation capacities suggesting their consideration as an alternate source for regenerative treatments.

Observing clonogenic, multipotent cells resident within the matrix of CB is not surprising given the need for rapid expansion during development. Similarly, stromal cells of the BM support the hematopoietic system and are required to carry out numerous roles in signaling, migration, and homing. It would be logical to expect BM stromal cells to contain a subset of active stem cells to facilitate this maintenance; however, they appear to occur at lower incidence than cells within CB. The reported proliferative output and developmental potential of MSCs is varied across the lineages obtained, related to the site and age of cells isolated;[20,21] however, the greatest variation of results is intrinsically determined by the isolation methodology. The true identity of MSCs has often been obscured by different laboratories that employ different isolation and in vitro culture methods. These variables are responsible for the diverse phenotype and function of described cell populations. Here, BM and CB cells were harvested from long bones following the removal of connective tissue and complete abrasion of the periosteum, with BM released from the canals by combined crushing and flushing, followed by density centrifugation for MNC isolation. Cells were liberated from segmented CB pieces by proteolytic digestion of the matrix following the crushing. Elimination of the periosteal layers and

incorporated vasculature was an essential step in our methodology to demonstrate that subsequently isolated stromal cells were originally resident within the compact ECM of CB or along the inner, endosteal lining. Parallel studies from our laboratory have demonstrated the identification and subsequent clonal capacity of BM-derived MSC subsets with a stringent and gentler tissue dissociation procedure than is typically applied to BM harvests;[22] however, based on the isolation methodologies reported in this study, which reflect more standard and accepted BM-MSC isolation, our results indicate that cells resident within calcified CB are the more potent MSC reserve.

By absolute cell yields, we observed the BM as a more abundant cell source for the isolation of candidate MSC; however, the CB contained a higher incidence per cell yield of recovered clonogenic stromal cells. The composition of CFU-F from CB and BM indicated both quantitative and qualitative differences in clonal capacity; not only did CB contain more colonies within the unfractionated tissues, the lineage depletion retained 50% of total CFU-F. Conversely for BM, lineage depletion removed 99.5% of total cells yet recovered <1% of CFU-F. The per-cell incidence of BM CFU-F was doubled in lineage-depleted cells; however, this is in stride with typical BM harvesting experiments. There are many colony forming cells within the compartment; however, typical attempts to isolate the stromal cells complement result in their elimination. Mononuclear and lineage-depleted BM also generated significantly fewer secondary colonies, with respect to serial plating efficiency, than analogous populations from CB. When the size and morphology of CFU-F were compared, a qualitative difference was observed, where eightfold or greater more CB colonies were scored as "large" compared to BM. CB also formed CFU-F that were compact and dense, with the classical cobblestone phenotype, demonstrating the secretion of abundant ECM proteins. These were predominantly a subset of the largest CFU-F, specifically those undergoing a spontaneous differentiation toward osteogenic, chondrogenic, and adipogenic lineages that were almost exclusively restricted to the CB compartment. Under inductive in vitro conditions, CB-MSCs demonstrated enhanced lineage-specific differentiation. This was observed in both polyclonal bulk culture and single-cell-derived colony outgrowth. The differentiation potential of cells isolated from BM was commonly more limited to the bone lineage and contrasted with CB-MSCs, which readily produced all three lineages of bone, cartilage, and adipose. Interestingly, when differentiated colonies were scored for their morphology, bone was consistently the most common lineage, and though no single BM-derived clone was observed to form all three lineages, 11% of CFU-F from CB demonstrated tri-potential.

MSC studies have increasingly attempted to characterize cells to distinguish MSCs from bulk populations by surface antigens; however, this is predominantly on cultured cells and not prospectively on fresh isolates. Certain stromal markers have been commonly described although no consensus exists for a prototypical in vivo MSC panel. For example, CD90 (Thy-1), CD146 (melanoma cell adhesion molecule (MCAM)), and Stro-1 subpopulations from BM have been reported to be enriched for MSCs, but not the CD34+ subsets.[23,24] Conversely, several laboratories have reported that extra-skeletal MSCs derived from adipose tissue or the stromal-vascular fraction of lipoaspirates are included in a CD34+ population.[25,26] The apparent phenotypic differences in MSCs from different source tissues are undoubtedly related to the differences in the reported perivascular stem cell niche and microenvironment.[27,28] In this study, we utilized two well-described markers to identify clonogenic stromal cells, in combination with a depletion of all hematopoietic and vascular endothelial cells via a lineage panel. Initially, the depletion occurred with immunomagnetic bead separation prior to FACS; however, the efficacy was maintained by combining the lineage markers with CD45 and CD31 directly labeled in FACS, permitting more rapid isolation. Markers for stromal cell fractions, Thy-1 and VLA-1 were expressed on both BM- and CB-derived cells; however, the majority of these cells were within the Lin+ fraction. The Lin− fraction however revealed differential expression from the bone compartments, further demonstrating the disparity observed in the clonal proliferation. Although the Lin− BM did contain cells expressing low levels of either Thy-1 or VLA-1, we observed that the Lin−/CD45−/CD31−/VLA-1+/Thy-1+ phenotype was solely restricted to CB isolates and further, when single cells were plated, it enriched for the production of large tri-potent colonies. It should be noted that as a consequence of the project milestones associated with this study, and despite the phenotype's promising attributes, the low frequency (~1/11,000) made this subpopulation unfeasible to assay in further clonal studies and employ in downstream in vivo transplants although bulk isolates still validated that CB-MSCs had statistically significantly greater capacity to support the formation of bone tissue than BM-MSCs.

Although clearly more potent, CB-MSCs comprised a limited and lower absolute cell yield, presenting a greater obstruction for physical isolation from autologous sites, a contributing reason why BM is readily harvested and expanded as the source of MSC for therapies. This leads to considerations of priority; whether the most potent source of cells, which are also more readily expanded ex vivo, are the primary target for therapy or whether sheer cell number and ease of access are preferred for a patient, to provide a more immediate clinically applicable solution. The advantages of CB over BM cells reported in this study are relevant to the MSC field. CB may be considered a viable alternative to BM for adult stem cell therapies considering their reported capacity to modulate host immune responses which would theoretically permit exogenous, allogeneic CB-MSCs as a therapeutic option. Cells supplied by healthy donors (familial or banked) could be expanded and

cryogenically stored until application, alleviating the issue of low fresh cell dosage and allowing cells to be applied in an "off-the-shelf" manner—reducing the requirement for autologous cells in particular treatments. The question of potency versus dose suggests CB as a viable cell source if suitably expanded ex vivo although limited when autologous or freshly obtained. Looking at further studies, additional alternatives are extra-skeletal MSC sources. For example, tissues of mesodermal ontological origin which are more accessible and abundant than bone, permitting cell isolation with minimal invasiveness or additional patient trauma. Dermis and adipose tissue contain their own resident candidate MSCs that can be harvested for research and clinical use, which we have examined in other studies (dermis; D.B., adipose; M.B.M., unpublished data). Exploiting the relative ease for accessibility and donor site availability provides an additional benefit of increased MSC yield—permitting autologous use of a patient's cells with reduced need for ex vivo cell expansion. These alternatives provide both high yield and defined phenotypically enriched fractions, with improved clonogenic potency over BM, as has been shown here with CB.

Experimental procedures

Isolation of BM and CB cells

Male Sprague-Dawley rats (200–250 g) were sacrificed by carbon dioxide inhalation after isofluorane sedation. Tibiae and femora were dissected and cleaned rigorously with a sterile scalpel to remove muscle, tendon, and the periosteum. The marrow was recovered by segmentation of the bones, flushing the canal with phosphate-buffered saline (PBS), and crushing the bones using a mortar and pestle with five PBS washes. Total marrow isolate was collected by centrifugation and re-suspended in PBS. Mononuclear cells were isolated by centrifugation following a 2:1 overlay on Ficoll, at $150 \times g$ for 30 min at room temperature without brake (Ficoll-Paque™ PLUS; Sigma Aldrich, St. Louis, MO, USA). CB cells were obtained via crushing in a mortar and pestle with several washes of PBS-2% fetal bovine serum (FBS) with gentle agitation to remove contaminating marrow cells (as assessed by the bones' white color), bone fragments were transferred to 100 mm Petri dishes and submerged in a 3-mg/mL solution of type-1 collagenase (CLS-1; Worthington Biochemical Corporation, Lakewood, NJ, USA) in PBS for 5 min. Fragments were chopped using a scalpel and transferred to a 50-mL polypropylene tube. A collagenase/dispase enzymatic solution was added: 3 mg/mL collagenase, 4 mg/mL dispase II (Roche, Indianapolis, IN, USA) at 2 mL per bone, and the tube incubated on a 37°C shaking platform at 250 r/min for 45 min. Following digestion, the volume was doubled with PBS-2% FBS and bone fragments were allowed to settle for 5 min prior to collection of supernatant. This process was repeated to ensure maximal cell recovery and to remove bone debris. The resultant cell suspension was filtered through successive 70 and 40 µm nylon cell strainers (BD Falcon, Bedford, MA, USA) with washes at $400 \times g$ for 5 min at 4°C and supernatant transferred into fresh tubes and spun again to ensure maximal cell recovery.

Lineage depletion and FACS

Cell populations were depleted of cells expressing antigens for hematopoietic and vascular endothelial lineage-committed cells by negative immunomagnetic selection using Dynabeads (Dynal Biotech ASA, Oslo, Norway). A lineage panel of markers was assembled with purified mouse anti-rat antibodies for CD2, CD3, CD4, CD8, CD18, CD11b/c, CD45RA, CD71, Gr(RP-1), and Mono/Mac (BD Pharmingen, San Diego, CA). The mixed lineage cocktail contained antibodies at a 1/500 dilution with 10 µL used per 10^6 cells, and following labeling were incubated with sheep anti-mouse Dynabeads at a ratio of 10 beads/cell. Dynabeads were added to the cells in two rounds of depletion, placed on a Dynal magnetic particle concentrator (MPC)-L magnet for 1 min to facilitate clearance of bead-bound lineage positive cells. Unbound lineage negative cells were collected and counted to assess efficacy of depletion. Markers used for further phenotypic fractionation were CD31-PE, CD45-PE-Cy5, Thy-1-PerCP (CD90), and purified hamster VLA-1 (CD49a) with a secondary goat anti-hamster IgG-fluorescein isothiocyanate (FITC; Jackson ImmunoResearch, West Grove, PA, USA). Cells were labeled and re-suspended in PBS-2% FBS containing the viability dye Fluorogold (Fluorochrome; LLC, Denver, CO, USA). Flow cytometry was performed on a BD FACSAria cell sorter (BD Biosciences, San Jose, CA, USA).

Cell culture and CFU-F plating and assessment

Cells were cultured in α-minimum essential medium (MEM) with 20% (v/v) human MSC-grade FBS (Hyclone, South Logan, UT, USA) at 37°C under low oxygen tension conditions (incubator: 5% O_2, 10% CO_2, and 85% N_2; Forma Scientific, Marjetta, OH, USA). For colony assays, cells were seeded in six-well plates at serial densities from 1 to 5×10^5 cells/well for 10 days. Wells were fixed and stained in PBS with a 2% formalin/0.5% toluidine blue solution for 2 h. CFU-F were scored by size; designated as small (50–5000 cells) or large (>5000 cells), corresponding to ~1–3 and ≥3 mm colony diameter, respectively. Colonies demonstrating morphological signs of spontaneous differentiation were optionally detected with respective bone, cartilage, and fat differentiation stains, as further described below. Secondary colony forming potential was assessed by the serial plating of dispersed primary CFU-F at limiting dilution. Selected small and large colonies were isolated with a cloning ring, dissociated and harvested following treatment with trypsin (Gibco Invitrogen), and replated at two densities into full in six-well plates (a 3:1 split of the

primary CFU-F, each containing 75% or 25% of the total cells each). Following 14 days in low oxygen incubation, cells were fixed, stained, and scored as above.

In vitro differentiation assays for osteogenic, chondrogenic, and adipogenic induction

Osteogenic. Passage one cells were seeded at 10^3 cells/ well in 24-well plates and grown in basal α-MEM 20% fetal calf serum (FCS) to 80% confluence. Osteo-inductive media (base media supplemented with 10 nM dexamethasone, 100 μM ascorbate-2-phosphate, and 4 mM KH_2PO_4, all from Sigma Aldrich) were replaced every 3 days for duration of the 20-day assay. Wells were washed three times in PBS and fixed for 15 min in 10% buffered formalin. Wells were then rinsed briefly twice in distilled water and stained with Von Kossa's reagent (5% aqueous silver nitrate solution for 30 min under ultraviolet (UV) light, rinsed two times in distilled water and then covered with aqueous 5% sodium thiosulfate for 5 min) and for AP activity (as per the VECTOR Blue Alkaline Phosphatase Substrate Kit, Vector Labs, Burlingame, CA, USA).

Chondrogenic. Cells were seeded in six-well plates at a density of 5×10^4 cells/well and grown in basal α-MEM 20% FCS media for 3–5 days until in log phase. Following trypsinization and cell counts, 4×10^5 passage one cells were pelleted at $300 \times g$ into 15 mL tubes to promote micromass pellet formation. Cells were then covered in 1 mL of chondro-inductive media (α-MEM serum-deprived base media with 10% bovine serum albumin (BSA), 0.01 mg/mL recombinant human insulin, 0.2 mg/mL transferrin, and 0.24% low-density lipoprotein solution), supplemented with 10 ng/mL transforming growth factor (TGF)-β_3, 10 ng/mL BMP-6, and 50 ng/mL platelet-derived growth factor-BB (PDGF-BB; all from R&D Systems, Minneapolis, MN, USA). Media were aspirated and replaced every 3 days for the 21-day assay duration at which point pellets were washed in PBS, fixed in Zinc formalin (0.75% $ZnCl_2$, 2.5% formalin), and rehydrated before paraffin embedding. Sections of pellets were stained for cartilage matrix proteoglycans by alcian blue (1% (w/v) alcian blue 8GX in aqueous HCl pH 1.0 and 1 M $MgCl_2$, for 30 min followed by rinses in 0.1 N HCl and counterstained with nuclear fast red) and toluidine blue (0.1% (w/v) solution of toluidine blue in 1:1 isopropanol:water, for 2 min followed by a wash in water and rapid dehydration).

Adipogenic. Passage one cells were seeded at 10^3 cells/ well in 24-well plates and grown in basal α-MEM 20% FCS until reaching >90% confluence. Adipo-inductive media were added for a period of 3 days (Dulbecco's modified Eagle's medium (DMEM) supplemented with 10% (v/v) horse serum (Gibco Invitrogen) and the addition of 10 nM hydrocortisone, 60 μM indomethacin, and 500 μM 1-isobutyl-3-methylxanthine, all from Sigma Aldrich).

Following the inductive period, base media of DMEM 10% horse serum was replaced every 3 days. Wells were washed three times in PBS and fixed for 15 min in 10% buffered formalin. Wells were then rinsed in water followed by 60% isopropanol and stained with Oil Red O (prepared several hours earlier, 0.5% (w/v) Oil Red O in isopropanol mixed 6:4 with distilled H_2O, filtered through blotting paper). Wells were stained for 10 min, followed by a rinse in 60% isopropanol and washes in water with hematoxylin counterstain.

In vivo transplants for bone formation

Cells were isolated from the BM and CB compartments of male Lewis rats (125–150 g) as described above. Primary cells were plated in T-75 cm^2 flasks to reach log phase growth after 7–10 days of culture. To assess the in vivo bone-forming capacity of donor cells, porous collagen sponges were loaded with 2×10^5 cells ± 500 ng BMP-2-loaded microparticles, as previously described[29,30] and doses of BM or CB cells, followed by surgical implantation into recipient rats. Briefly, collagen sponges were fabricated from Type-I collagen (bovine; Sigma Aldrich) in 0.05 M acetic acid to a final concentration of 0.5% by weight, cast in aluminum trays and frozen to −10°C an average cooling rate of 0.3°C/min. Collagen sheets were then lyophilized and dehydrothermal (DHT) crosslinked overnight (105°C in vacuum oven). Using a 1-cm biopsy punch, individual scaffolds were cut from the dried collagen sheets. Scaffolds were chemically crosslinked in 70% ethanol containing 1-ethyl-3-(3-dimethylaminopropyl)-carbodiimide (EDC) and N-hydroxysuccinimide (NHS) at a ratio of 1:1:5 EDC:NHS: –COOH (0.0012 mol –COOH/g collagen) for a minimum of 2 h. Scaffolds were sterilized in ethylene oxide gas and stored at room temperature. Scanning electron microscopy (SEM) was used to confirm uniform, interconnected pores with diameters from 200 to 500 μm. Recombinant human BMP-2 (R&D Systems) of 100 μg was passively loaded into 8×10^7 oxidized porous silicon (pSi) microparticles in a 2-mL PBS solution. Loaded pSi particles were then coated with poly(lactic-co-glycolic acid) (PLGA) using a modified solid in oil in water emulsion method as mentioned in our previous studies (28, 29). Cells and PLGA/pSi microparticles were loaded into the collagen sponges using a fibrin-based gel. Briefly, cells and microparticles were suspended in a solution containing 3 mg/mL fibrinogen (bovine fibrinogen, Sigma Aldrich) in PBS. The solutions were prepared such that 75 μL contained the 200,000 cells, 500 ng BMP-2-loaded microparticles, and fibrinogen. A second solution was prepared with 100 U/mL bovine thrombin (BioPharm Laboratories, Bluffdale, UT, USA). These solutions were warmed to 37°C, co-injected into the scaffolds (that contain a 200-μL void volume), and placed in incubator for 5 min as the fibrin set and then washed in PBS. Unloaded

cells were counted by hemocytometer. Empty collagen scaffolds were used as a negative control. Scaffolds were incubated overnight in osteogenic media and implanted in subcutaneous pouches on the back flanks of male Lewis rats (150–200 g). Implant scaffolds were washed twice in sterile PBS for 10 min prior to implantation. Rats were anesthetized by inhalation of 5% isoflurane in O_2 through a rebreather mask. A 2-cm incision was prepared through the dermis alongside the spine and three scaffolds were placed in pockets of each flank with at least 1 cm spacing between each implant. Following the implantation of the scaffolds in a non-sequential (randomized treatment) manner, wounds were closed with skin clips. All experimental groups were performed in quadruplicate (n = 4). Procedures were performed under the approved protocol of the Institutional Animal Care and Use Committee at UT-HSC.

Histological processing and analysis

Scaffolds were excised from sacrificed rats, fixed in 10% neutral buffered formalin for 2 h and paraffin embedded for histology. Sections were stained with H&E, OPN, and GT. H&E and GT stains were performed as per standard methodology. OPN was detected by immunoperoxidase staining with a monoclonal biotinylated goat anti-mouse antibody (cross reactive to rat; R&D Systems) at 5 µg/mL for 1 h. Sections were washed and incubated with a secondary horseradish peroxidase (HRP)-conjugated anti-goat antibody (Jackson ImmunoResearch) and detected by 3,3′-diaminobenzidine (DAB) substrate. Quantitation of bone formation was performed on micrographs taken with a Nikon Eclipse 90i light microscope at 10× and 20× magnifications. The percentage of implant area scored as positive for calcified collagen deposition or active OPN was calculated by Nikon NIS-Elements software. Values were averaged from three non-serial sections of n = 4 scaffolds per experimental group. Standard deviation and error within groups and statistical significance between groups were calculated with analysis of variance (ANOVA) using Origin Pro 8.5 statistics software.

References

1. Friedenstein AJ, Petrakova KV, Kurolesova AI, et al. Heterotopic of bone marrow. Analysis of precursor cells for osteogenic and hematopoietic tissues. *Transplantation* 1968; 6(2): 230–247.
2. Caplan AI. Mesenchymal stem cells. *J Orthop Res* 1991; 9(5): 641–650.
3. Pittenger MF, Mackay AM, Beck SC, et al. Multilineage potential of adult human mesenchymal stem cells. *Science* 1999; 284(5411): 143–147.
4. Baksh D, Song L and Tuan RS. Adult mesenchymal stem cells: characterization, differentiation, and application in cell and gene therapy. *J Cell Mol Med* 2004; 8(3): 301–316.
5. Meirelles LDS, Chagastelles PC and Nardi NB. Mesenchymal stem cells reside in virtually all post-natal organs and tissues. *J Cell Sci* 2006; 119(11): 2204–2213.
6. Covas DT, Panepucci RA, Fontes AM, et al. Multipotent mesenchymal stromal cells obtained from diverse human tissues share functional properties and gene-expression profile with CD146+ perivascular cells and fibroblasts. *Exp Hematol* 2008; 36(5): 642–654.
7. Murphy MB, Moncivais K and Caplan AI. Mesenchymal stem cells: environmentally responsive therapeutics for regenerative medicine. *Exp Mol Med* 2013; 45: e54.
8. Salem HK and Thiemermann C. Mesenchymal stromal cells: current understanding and clinical status. *Stem Cells* 2010; 28(3): 585–596.
9. Dominici M, Le Blanc K, Mueller I, et al. Minimal criteria for defining multipotent mesenchymal stromal cells. The International Society for Cellular Therapy position statement. *Cytotherapy* 2006; 8(4): 315–317.
10. Corradetti B, Taraballi F, Powell, et al. Osteoprogenitor cells from bone marrow and cortical bone: understanding how the environment affects their fate. *Stem Cells and Development* 2014; 24(9): 1112–1123.
11. Brouard N, Driessen R, Short B, et al. G-CSF increases mesenchymal precursor cell numbers in the bone marrow via an indirect mechanism involving osteoclast-mediated bone resorption. *Stem Cell Res* 2010; 5(1): 65–75.
12. Short BJ, Brouard N and Simmons PJ. Prospective isolation of mesenchymal stem cells from mouse compact bone. *Methods Mol Biol* 2009; 482: 259–268.
13. Murphy MB, Blashki D, Buchanan RM, et al. Engineering a better way to heal broken bones. *Chem Eng Prog* 2010; 106(11): 37–43.
14. Patel DM, Shah J and Srivastava AS. Therapeutic potential of mesenchymal stem cells in regenerative medicine. *Stem Cells Int* 2013; 2013: 496218.
15. Prockop DJ, Kota DJ, Bazhanov N, et al. Evolving paradigms for repair of tissues by adult stem/progenitor cells (MSCs). *J Cell Mol Med* 2010; 14(9): 2190–2199.
16. Bianco P, Cao X, Frenette PS, et al. The meaning, the sense and the significance: translating the science of mesenchymal stem cells into medicine. *Nat Med* 2013; 19(1): 35–42.
17. Krasnodembskaya A, Song Y, Fang X, et al. Antibacterial effect of human mesenchymal stem cells is mediated in part from secretion of the antimicrobial peptide LL-37. *Stem Cells* 2010; 28(12): 2229–2238.
18. Ryan JM, Barry FP, Murphy JM, et al. Mesenchymal stem cells avoid allogeneic rejection. *J Inflamm* 2005; 2: 8.

19. Law S and Chaudhuri S. Mesenchymal stem cell and regenerative medicine: regeneration versus immunomodulatory challenges. *Am J Stem Cells* 2013; 2(1): 22–38.

20. Baxter MA, Wynn RF, Jowitt SN, et al. Study of telomere length reveals rapid aging of human marrow stromal cells following in vitro expansion. *Stem Cells* 2004; 22(5): 675–682.

21. Muraglia A, Cancedda R and Quarto R. Clonal mesenchymal progenitors from human bone marrow differentiate in vitro according to a hierarchical model. *J Cell Sci* 2000; 113(Pt 7): 1161–1166.

22. Suire C, Brouard N, Hirschi K, et al. Isolation of the stromal-vascular fraction of mouse bone marrow markedly enhances the yield of clonogenic stromal progenitors. *Blood* 2012; 119(11): e86–e95.

23. Baksh D, Yao R and Tuan RS. Comparison of proliferative and multilineage differentiation potential of human mesenchymal stem cells derived from umbilical cord and bone marrow. *Stem Cells* 2007; 25(6): 1384–1392.

24. Gronthos S, Graves SE, Ohta S, et al. The STRO-1+fraction of adult human bone marrow contains the osteogenic precursors. *Blood* 1994; 84(12): 4164–4173.

25. Mitchell JB, McIntosh K, Zvonic S, et al. Immunophenotype of human adipose-derived cells: temporal changes in stromal-associated and stem cell-associated markers. *Stem Cells* 2006; 24(2): 376–385.

26. Traktuev DO, Merfeld-Clauss S, Li J, et al. A population of multipotent CD34-positive adipose stromal cells share pericyte and mesenchymal surface markers, reside in a periendothelial location, and stabilize endothelial networks. *Circ Res* 2008; 102(1): 77–85.

27. Crisan M, Yap S, Casteilla L, et al. A perivascular origin for mesenchymal stem cells in multiple human organs. *Cell Stem Cell* 2008; 3(3): 301–313.

28. Kuhn NZ and Tuan RS. Regulation of stemness and stem cell niche of mesenchymal stem cells: implications in tumorigenesis and metastasis. *J Cell Physiol* 2010; 222(2): 268–277.

29. Murphy M, Blashki D, Buchanan R, et al. Multi-composite bioactive osteogenic sponges featuring mesenchymal stem cells, platelet-rich plasma, nanoporous silicon enclosures, and peptide amphiphiles for rapid bone regeneration. *J Funct Biomater* 2011; 2(2): 39–66.

30. Fan D, De Rosa E, Murphy MB, et al. Mesoporous silicon-PLGA composite microspheres for the double controlled release of biomolecules for orthopedic tissue engineering. *Adv Funct Mater* 2012; 22(2): 282–293.